Chinese Journal of Chemical Engineering 48 (2022) 158–165

Contents lists available at ScienceDirect

Chinese Journal of Chemical Engineering

journal homepage: www.elsevier.com/locate/CJChE

Full Length Article

A route for the study on mass transfer enhancement by adding particles in liquid phase

Xing Su [1], Ning Qiao [2,3], Bao-Chang Sun [2,3,*]

[1] College of Chemical and Material Engineering, Quzhou University, Quzhou 324000, China
[2] State Key Laboratory of Organic-Inorganic Composites, Beijing University of Chemical Technology, Beijing 100029, China
[3] Research Center of the Ministry of Education for High Gravity Engineering and Technology, Beijing University of Chemical Technology, Beijing 100029, China

ARTICLE INFO

Article history:
Received 1 April 2022
Received in revised form 27 May 2022
Accepted 31 May 2022
Available online 3 June 2022

Keywords:
Mass transfer
Hydrogen
Water
Methanol
Activated carbon

ABSTRACT

This work presents a route for the study on the absorption performance of gas into liquid under the condition of adding particles in a stirred constant temperature reactor. Two evaluated systems, hydrogen–water and hydrogen–methanol, with the addition of activated carbon particles (ACP) were carried out, respectively. The results showed that the addition of ACP into the water can enhance the mass transfer between hydrogen and water, the enhancement factor increases rapidly with the increase of the ACP content, and then tends to be unchanged. However, for the hydrogen–methanol system, ACP has little effect on the mass transfer performance. In addition, a gas–liquid mass transfer model considering the effect of solid particle enhancement was established based on the shuttle effect and two-film model. Results indicated that the predicted value agreed well with the experimental value in both hydrogen–methanol–ACP and hydrogen–water–ACP systems.

1. Introduction

Gas–liquid–solid three-phase reactions are very common in the chemical industry, such as fermentation [1,2], hydrogenation [3–6], oxidation, and usually, the gas–liquid mass transfer process is the limiting step for the whole process, therefore, the enhancement of gas–liquid mass transfer is desired for improvement of process efficiency in industry.

Many studies have explored the absorption performance of solid particles in liquid phases. Tinge *et al.* [7] studied the effect of activated carbon particles (ACP) on the rate of propane and ethane absorption in water in a stirred tank, and found that ACP can increase the gas–liquid mass transfer coefficient up to 3.5 times. Alper *et al.* [8] studied oxygen absorption in a slurry solution containing ACP, and found that the oxygen absorption rate increased 3 times compared to that without ACP. Ozkan *et al.* [9] studied the effect of ACP, kieselguhr, Fe_2O_3 and $BaSO_4$ on the rate of oxygen absorption in water, respectively, and illustrated that all the particles can significantly enhance the absorption rate of oxygen in the water. However, most of the studies were focused on the intensification performance by adding solid particles, whereas researches on the methodology and exact mechanism of mass transfer near the gas–liquid interface are still rare.

It has been reported that the mechanism of dispersed phase enhancing gas–liquid mass transfer in stirred tanks mainly involve the shuttle effect [8,10] and hydrodynamic effect [11]. Demmink *et al.* [12–13] performed C_2H_4, C_2H_2, and H_2S enhanced absorption experiments with newly generated S particles. Based on the surface renewal theory and the shuttle hydrodynamic effect, a model was established. The experimental results showed that the model can predict the intensification performance by adding ACP and ultrafine TiO_2 particles into several aqueous solutions [12,14]. Brilman *et al.* [15] proposed a one-dimensional heterogeneous and non-stationary mass transfer model based on the shuttle effect and penetration model. It was concluded that only the particles being closed to gas–liquid interface can enhance the absorption performance and suggested that two- and three-dimensional models should be developed to better investigate near interface effects. Zhang *et al.* [16] also developed a general mass transfer enhancement factor model (GEFM) which was based on the shuttle effect and hydrodynamics effect to calculate the overall enhancement factor of mass transfer in the presence of dispersed particles. As mentioned above, modeling for the prediction of absorption enhancement factor has been widely applicated, nevertheless, most of them were usually simplified by using an average mass transfer coefficient instead of the varied one near the gas–liquid

* Corresponding author at: No 15 Bei San Huan Dong Road, Beijing 100029, China.
E-mail address: sunbc@mail.buct.edu.cn (B.-C. Sun).

https://doi.org/10.1016/j.cjche.2022.05.013
1004-9541/

interface. Consequently, further theoretical investigations often suffered from lacking of a study approach for the determination of the varied gas mass transfer coefficients in gas–liquid–solid three-phase systems, especially when no experimental data are available.

The aim of this study is to propose a new route for the study on mass transfer enhancement in liquid-containing dispersed particles. Firstly, a device for measuring gas solubility in gas–liquid–solid three-phase systems was designed based on an indirect method by gas phase pressure change. The testing method was verified and a calculation method for gas mass transfer coefficient was then obtained. Secondly, the effect of ACP on the mass transfer of hydrogen in methanol and in water was investigated, respectively. Based on the shuttle effect and two-film model, a three-dimensional unsteady heterogeneous mass transfer model for enhancing gas–liquid mass transfer was established and validated by comparison with the experimental data. The effects of operating conditions such as the distance between the particle and the gas–liquid interface L, the distribution coefficient m, the concentration m_S, and the residence time τ on the enhancement factor E were analyzed.

2. Experimental

2.1. Experimental procedure

The experiment setup for measuring gas solubility and liquid volume mass transfer coefficients in liquid is schematically shown in Fig. 1. It mainly consists of a hydrogen cylinder, equilibrium chamber, gas chamber, thermostatic water bath and magnetic stirrer, and vacuum pump. The gas chamber with a volume of 273 ml was used as a buffer tank and put in the water bath for preheating in advance. The magnetic stirring devices were arranged under the equilibrium chamber and the gas chamber, respectively. Pressure transmitters (Keller 33x, Switzerland; 0–10 MPa, 0.05%) were connected to the upper part of the equilibrium chamber and the gas chamber, which can record the pressure in the two chambers in real time. The temperature of the equilibrium chamber and the gas chamber were both controlled by the water bath, and the temperature control accuracy of the water bath is ±0.05 °C. Gas–liquid mass transfer occurred in the equilibrium chamber, and its volume is 140 ml.

Additionally, in order to exclude the influence of temperature change on gas pressure, the following requirements were made for the measuring device. (a) The accuracy of temperature control should be within ±0.1 °C. According to the ideal gas equation of state (at 1 MPa and 30 °C), when temperature changes by 1 °C, the gas pressure will change by 3 kPa. In this paper, we want to study the effect of particles on H_2 solubility and liquid volume mass transfer coefficient, and this effect could be very small; (b) the gas should be sufficiently preheated to the experimental temperature in the gas chamber 4.

To test the reliability of the device, the solubility of H_2 in toluene was firstly tested with the device at 25 °C and the results were compared with literature data [17], as shown in Table 1. It was found that the maximum error was only 1.1%.

The experimental process can be briefly described as follows: Evacuated the entire system, and closed all valves after evacuating. The degassed solution entered the equilibrium chamber through a buret from valve 6. The amount of solution entering the equilibrium chamber was obtained by reading before and after the buret, and the liquid temperature in the buret was measured at the same time to estimate the change of the amount of solution. Filled the gas chamber with hydrogen from the hydrogen cylinder. Turned on the heating and stirring, and kept the system stable for 1 h after reaching the set temperature. Stopped stirring, at this time, the pressure of the equilibrium chamber was recorded as p_0. Opened the valve 8 to slowly fill the equilibrium chamber with hydrogen from the gas chamber, and closed the valve 8 after the pressure of the equilibrium chamber reached p_1. Turned on the agitation and recorded the pressure changes over time. When the pressure was not changing, recorded the pressure in the equilibrium chamber, the pressure in the equilibrium chamber was recorded as p_2.

The ACP used in the experiment was purchased from Xianfeng Company (Nanjing, China), and its main properties were listed in Table 2. Hydrogen was purchased from Haipu Company (Beijing, China) with a purity of 99.999%.

2.2. Determination of liquid volume mass transfer coefficient

Based on the parameters obtained from experiments mentioned above, the method for determination of liquid volume mass transfer coefficient is described as follows:

The mass transfer coefficient of the liquid phase was measured by the gas intermittent absorption technique. The principle of the gas intermittent absorption technique is to transform the measurement of liquid phase concentration into the measurement of gas phase pressure according to the classic two-film theory. When deriving the expression of liquid volume mass transfer coefficient, the basic assumptions were made as follows: (1) the absorption of gas in liquid can be described by Henry's law, due to the relatively low hydrogen solubility in liquid at low pressure; (2) when filling the equilibrium chamber with hydrogen from the gas chamber, the gas absorption in liquid before the start of stirring can be neglected; (3) the gas phase and liquid phase temperatures in the equilibrium chamber can be considered to be uniform and constant, because the changes of gas pressure and liquid concentration were both extremely minor during the experimental process; (4) mass transfer resistance in gas phase was ignored due to only pure gas was used; (5) the liquid phase can be considered to mix uniformly in the equilibrium chamber and have a uniform concentration at any time when the rotation rate was greater than or equal to 500 r·min^{-1} according to previous experiments; (6) phase interface instantly reached the phase equilibrium. According to the above assumptions, the derivation process of the liquid volume mass transfer coefficient was as follows:

The absorption rate of gas is equal to the rate at which the gas phase pressure decreases:

$$\frac{\mathrm{d}p}{\mathrm{d}t}=\frac{RT}{V_G}\frac{\mathrm{d}N_G}{\mathrm{d}t}=-\frac{RT}{V_G}\frac{\mathrm{d}N_L}{\mathrm{d}t} \tag{1}$$

According to the two-film theory, the differential mass equilibrium equation of the liquid phase is as follows:

$$\frac{\mathrm{d}N_L}{\mathrm{d}t}=V_L k_L a(c^*-c_L) \tag{2}$$

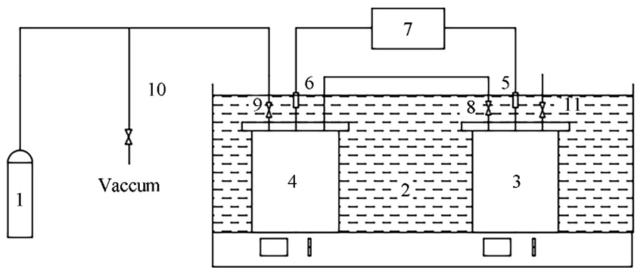

Fig. 1. Schematic of the experimental setup: (1) hydrogen cylinder, (2) thermostatic water bath and magnetic stirrer, (3) equilibrium chamber, (4) gas chamber, (5, 6) pressure transmitter, (7) computer, (8–11) valve.

Table 1
Comparison of experimental value and literature value

Pressure/MPa	Experimental solubility/%	Literature value, x/%	Error/%
1.0042	0.3067	0.3100	1.1
1.0040	0.3078	0.3100	0.7
1.0049	0.3089	0.3103	0.4
1.0029	0.3091	0.3096	0.2

According to Henry's law, the solubility of gas at low pressure is directly proportional to the partial pressure of the gas. The Henry constant is only related to temperature.

$$c^* = \frac{p}{H} \tag{3}$$

According to assumption (6), the concentration at gas–liquid interface is equal to:

$$c_{\mathrm{Li}} \approx c^* \tag{4}$$

Then the concentration in liquid bulk can be calculated by:

$$c_{\mathrm{L}} = \frac{N_{\mathrm{L}}}{V_{\mathrm{L}}} \tag{5}$$

Substituting Eqs. (3) and (5) to Eq. (2) can obtain the following equation:

$$\frac{\mathrm{d}N_{\mathrm{L}}}{\mathrm{d}t} = V_{\mathrm{L}} k_{\mathrm{L}} a \left(\frac{p}{H} - \frac{N_{\mathrm{L}}}{V_{\mathrm{L}}}\right) \tag{6}$$

The boundary conditions of Eq. (1) are: t = 0, p=p_i, N_{L} = 0, then the following integral equation can be obtained, where p_i is the initial pressure in the equilibrium chamber after inflation of gas.

$$N_{\mathrm{L}} = \frac{V_{\mathrm{G}}}{RT}(p_i - p) \tag{7}$$

Substituting Eqs. (1) and (7) into Eq. (6), we can get:

$$-\frac{\mathrm{d}p}{\mathrm{d}t} = k_{\mathrm{L}} a[(\alpha + 1)p - p_i] \tag{8}$$

where $\alpha = \frac{V_{\mathrm{L}}RT}{V_{\mathrm{G}}H}$.

Because, in equilibrium:

$$V_{\mathrm{L}}\frac{p_{\mathrm{f}}}{H} = \frac{V_{\mathrm{G}}}{RT}(p_i - p_{\mathrm{f}})$$

$$\frac{V_{\mathrm{L}}RT}{V_{\mathrm{G}}H} = \frac{p_i - p_{\mathrm{f}}}{p_{\mathrm{f}}} = \alpha$$

The integral of Eq. (8) is as follows:

$$\frac{p_{\mathrm{f}}}{p_i}\ln\frac{p - p_{\mathrm{f}}}{p_i} = k_{\mathrm{L}} a t \tag{9}$$

Considering the vapor pressure of the solvent, the final formula is:

$$\frac{p_2 - p_0}{p_1 - p_0}\ln\frac{p - p_2}{p_1 - p_0} = k_{\mathrm{L}} a t \tag{10}$$

If the left item of Eq. (10) is recorded as function, liquid volume mass transfer coefficient $k_{\mathrm{L}}a$ can be calculated by the linear slope of the function *vs t* plot.

Table 2
Properties of used ACP

Density/kg·m^{-3}	Diameter/μm	Surface area/m^2·g^{-1}
380	5	1800

Typical pressure changes with time were shown in Fig. 2. And the function-t plot was shown in Fig. 3. According to the value of slope in the fitting curve formula in Fig. 3, the liquid volume mass transfer coefficient $k_{\mathrm{L}}a$ can be obtained as 0.003301.

3. Model

In order to describe the effect of solid particles on the gas–liquid mass transfer process, different mass transfer enhancement models have been established, which mainly combined the classical gas–liquid mass transfer theory (two-film theory, permeability theory and surface renewal theory) with the mass transfer mechanism of gas adsorption in liquid in presence of solid particles (shuttle effect and hydrodynamic effect). The shuttle effect is that the dispersed phase can move into the liquid film under the entrainment of the fluid or Brownian motion, and stay in the film for a period of time. After adsorbing a certain amount of component to be transferred, the dispersed phase returns to the liquid bulk. The particles are regenerated after desorption and a transport process is completed. The hydrodynamic effect is that the dispersed particles in the multiphase system affect the hydrodynamics behavior of the system by colliding with the gas–liquid interface or inducing turbulence near the gas–liquid interface, resulting in the decrease of the diffusion layer thickness, thus enhancing the mass transfer.

On the basis of the shuttle effect and two-film model, a model of mass transfer enhancement by solid particles was established. The mass-transfer mechanism was shown in Fig. 4. First, the particles with adsorption ability move to the gas–liquid interface, and absorb gas components, then are transported by fluid to the liquid bulk to desorb, and this process cycles back and forth to achieve mass transfer enhancement. Based on the theories of hydrodynamics and mass transfer, the following assumptions were made:

(1) The concentration of dispersed particles in the gas–liquid interface is different from that in the bulk of the liquid phase. Langmuir isotherm adsorption equation can be used to describe the relationship between the two concentrations [18].

$$\Phi_{\mathrm{s}} = \Phi_{\mathrm{s,max}}\frac{k_{\mathrm{a}} m_{\mathrm{s}}}{1 + k_{\mathrm{a}} m_{\mathrm{s}}} \tag{11}$$

Φ_{s} and $\Phi_{\mathrm{s,max}}$ are the volume fraction of the dispersed particles in the gas–liquid interface and the maximum volume fraction in the liquid phase, respectively. And k_{a} is the adhesion coefficient. $\Phi_{\mathrm{s,max}}$

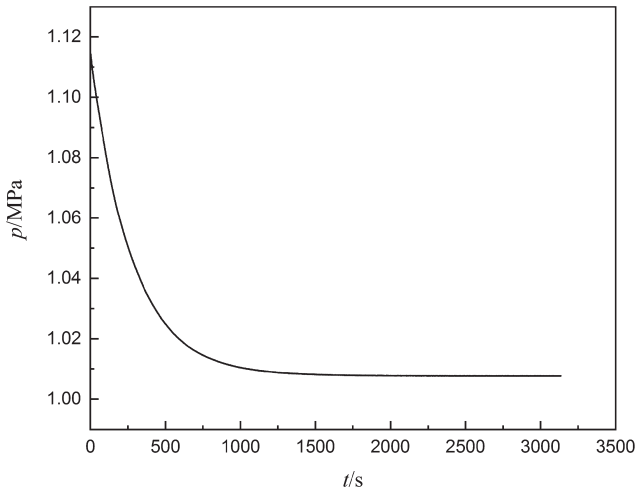

Fig. 2. Graph of pressure over time (H_2, 500 r·min^{-1}, 30 °C).

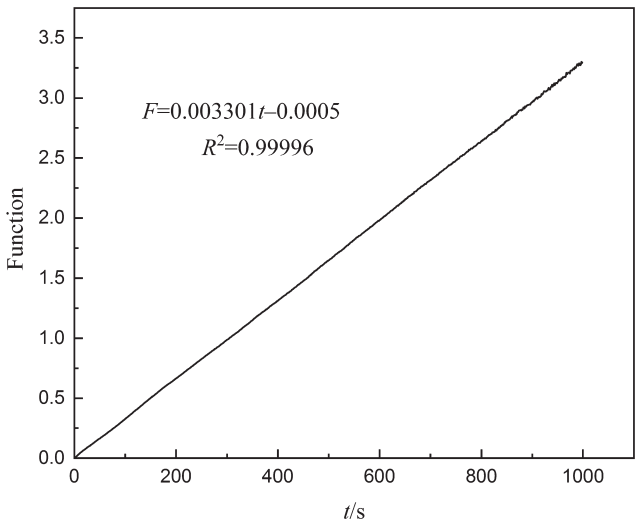

Fig. 3. Function-t graph (H_2, 500 r·min^{-1}, 30 °C).

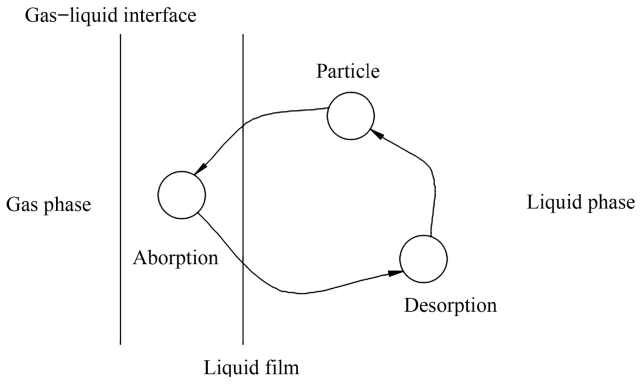

Fig. 4. Schematic diagram of mass transfer route.

and k_a are affected by stirring speed, particles size and wettability of particles.

(2) The theory of turbulence indicates that the contact time of gas and liquid can be estimated by the time scale of turbulent vortices [19]. Therefore, the residence time of the particles in the gas–liquid interface can be considered to be equal to the gas–liquid contact time.

$$\tau = \left(\frac{\nu}{\varepsilon}\right)^{1/2} \tag{12}$$

(3) The particles size in liquid phase is uniform, and the average particle size is adopted in this work.

The computational domain of this system was shown in Fig. 5. According to Nagy *et al.* [20], the distance L between the particles and the gas–liquid interface can vary between 0 and δ_x, where δ_x is the distance between adjacent particles which can be determined by $\delta_x = d(1/\Phi_s^{1/3}-1)$, where Φ_s is the particles volume fraction, d is the particles diameter. In these simulations, L was chosen as $\delta_x/2$ and the values of δ_x, δ_y and δ_z were all equal to $\delta_x + d$.

For continuous phase, the following equation can be obtained:

$$\frac{\partial c_A}{\partial t} = D_A\left(\frac{\partial^2 c_A}{\partial x^2} + \frac{\partial^2 c_A}{\partial y^2} + \frac{\partial^2 c_A}{\partial z^2}\right) \tag{13}$$

where c_A is the concentration of the component to be transferred in the continuous phase, D_A is the diffusion coefficient of the component in the liquid phase, which can be calculated by $D_A = D_0(\mu_0/\mu)$,

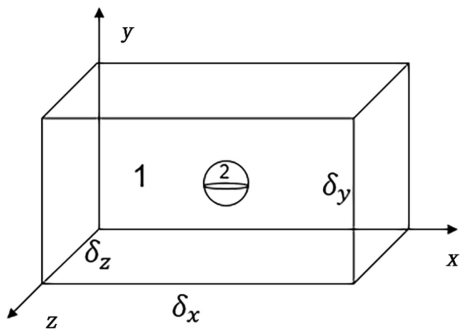

Fig. 5. Diagram of the model.

and D_0 is the diffusion coefficient of the components in the blank base liquid, μ_0 is the viscosity of blank base liquid, μ is the viscosity of continuous phase, which is calculated by $\mu = \mu_0(1 + 2.5\Phi_s)$ [21].

For the dispersed phase, the differential equation of $c_{A,d}$ can be described as follows:

$$\frac{\partial c_{A,d}}{\partial t} = D_{A,d}\left(\frac{\partial^2 c_{A,d}}{\partial x^2} + \frac{\partial^2 c_{A,d}}{\partial y^2} + \frac{\partial^2 c_{A,d}}{\partial z^2}\right) \tag{14}$$

Among them, $c_{A,d}$ is the concentration of the component in the dispersed phase, $D_{A,d}$ is the diffusion coefficient of the component in the dispersed phase.

The initial conditions for Eq. (14) are:

$$t = 0, x \geq 0, c_A = c_{A,d} = 0 \tag{15}$$

The boundary conditions for Eq. (15) are:

$$\begin{cases} t > 0,\ x = 0,\ c_A = c^* \\ x = \delta_x,\ c_A = 0 \\ y = 0 \ \text{or}\ y = \delta_y,\ \frac{\partial c_A}{\partial y} = 0 \\ z = 0 \ \text{or}\ z = \delta_z,\ \frac{\partial c_A}{\partial z} = 0 \end{cases}$$

where c^* is the concentration of the component in the gas–liquid interface, which can be obtained by Henry's Law: $c^* = p/H$, p is the absolute pressure of the gas, and H is Henry's coefficient.

The relationship between the boundary conditions on the interface of continuous phase and dispersed phase are as following:

$$D_A \nabla c_A = D_{A,d} \nabla c_{A,d} \tag{16}$$

$$c_{A,d} = m c_A \tag{17}$$

Among them, m is the distribution coefficient, indicating the adsorption capacity of dispersed particles.

Complex mass transfer differential equations and boundary conditions can be solved by numerical methods. Using the finite element method, we can get the gas concentration at any time and any position of the liquid in the system by the software of COMSOL Multiphysics 5.4. When the concentration distribution is obtained, the mass transfer flux J in the presence of nanoparticles can be obtained by the following formula:

$$J_A = \frac{1}{\tau S}\int_\tau \int_S -D_A \frac{\partial c_A}{\partial t}|_{x=0} \mathrm{d}A\mathrm{d}t \tag{18}$$

In the absence of particles, the mass transfer flux can be obtained by the following formula:

$$J_0 = \frac{1}{\tau S}\int_\tau \int_S -D_0 \frac{\partial c_A}{\partial t}|_{x=0} \mathrm{d}A\mathrm{d}t \tag{19}$$

Then, the enhancement factor can be expressed as:

$$E = \frac{J_A}{J_0} \tag{20}$$

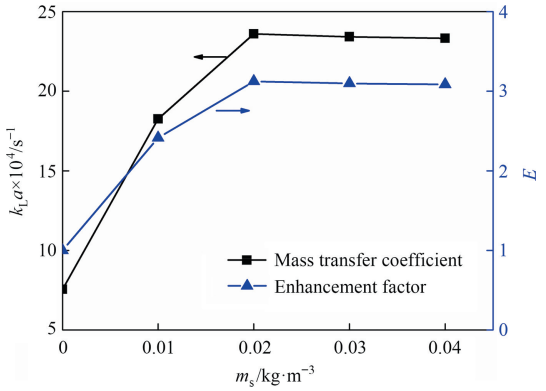

Fig. 6. Mass transfer coefficient of hydrogen absorption in water and the enhancement factor at different content of ACP (30 °C, 1 MPa, 500 r·min^{-1}).

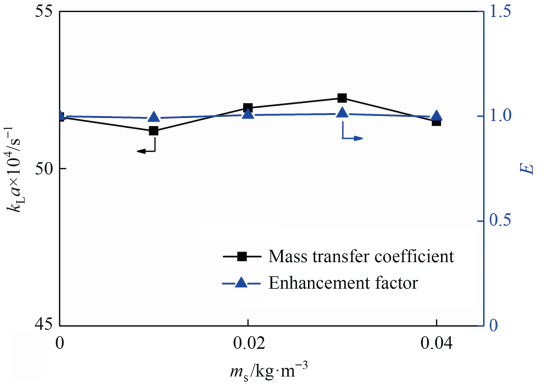

Fig. 7. Mass transfer coefficient of hydrogen absorption in methanol and the enhancement factor at different content of ACP (30 °C, 1 MPa, 500 r·min^{-1}).

4. Results and Analysis

4.1. Effect of solid content on mass transfer coefficient and enhancement factor

The influence of ACP content on the mass transfer coefficient and enhancement factor of hydrogen absorption in water and water–ACP system were shown in Fig. 6. It was illustrated that both the mass transfer coefficient and enhancement factor increase rapidly to about three higher times with the content of ACP increasing from 0 to 0.02 kg·m^{-3}, and then tends to level. The improved mass transfer performance can be mainly attributed to the gas adsorption by ACP and the shuttle effect. On the one hand, the hydrogen absorption capability of ACP is much greater than the solubility of hydrogen in water according to the very high distribution coefficient of hydrogen in water with ACP, which was reported as 140 by Dagaonkar *et al.* [22]. On the other hand, the ACP could move to the gas–liquid interface to absorb hydrogen, and then return to the liquid bulk to release hydrogen (the shuttle effect). Thus, due to the ACP constantly moved back and forth between the liquid film and the liquid bulk, resulting in the significantly enhanced gas–liquid mass transfer. However, because the enhanced mass transfer was also limited by the ACP content on the gas–liquid interface, which was not equal to that in the main body of liquid phrase, thus, when the ACP content increased to a certain value in the liquid bulk, the ACP content on the bubble surface reached its saturated amount, leading to the enhanced mass transfer performance became unchanged with the content of ACP higher than 0.02 kg·m^{-3}.

The influence of ACP content on the mass transfer coefficient and enhancement factor of hydrogen in methanol and methanol–ACP system were both shown in Fig. 7. It was demonstrated that the ACP have little effect on the mass transfer coefficient of hydrogen in methanol. Due to the distribution coefficient of hydrogen in methanol with ACP is as low as 22, obtained by Eq. (17), the effect of ACP on the solubility of hydrogen in methanol can be neglected, thus, the enhancing ability was limited. Besides, the hydrophobic property of the liquid can also influence the mass transfer coefficient. Wimmers *et al.* [23] studied the concentration distribution of ACP in ethanol aqueous solution at the gas–liquid interface as well as the main body of liquid phase. The adhesion ability of ACP on the bubble surface was found to be decreased with the increase of ethanol content in the ethanol aqueous solution. Therefore, for the ACP–methanol system, it can be deduced that the ACP in pure methanol is not as easily absorbed into the gas–liquid interface as that in water, because the properties of methanol are similar with ethanol rather than water, thus the ACP content near the gas–liquid interface could be lower in the ACP–methanol system, resulting in no promoting effect on the mass transfer of H_2 in methanol.

Table 3
Simulation parameters

	D_0/m^2·s^{-1}	$D_{A,d}$/m^2·s^{-1}	τ/s	m
Water	1.7332×10^{-9}	4×10^{-10}	0.029	140[22]
Methanol	3.0085×10^{-9}	4×10^{-10}	0.025	22

4.2. Comparison of experimental data and model

The parameters needed for mathematical model calculation were listed in Table 3.

Figs. 8 and 9 were the comparison of experimental results and model calculations in ACP–water system as well as in ACP–methanol system. It was revealed that the trends of experimental data were consistent well with the calculation results of the model in both systems. However, in Fig. 8, certain deviations between calculation and experiments occurred when the content of ACP increases to 0.02 and 0.03 kg·m^{-3}, which might be due to the errors during the experiment of measuring. All the experimental data were used to calculate the total standard deviation (SD) between the calculation and experiments by using the formula of Eq. (21), and the result turned out to be only 7.78%. In addition, it was shown in Fig. 10 that the deviations mainly came from the ACP–water system rather than ACP–methanol system, where the four data point in ACP–methanol system were happen to overlap so that they looked like one data point.

$$\mathrm{SD}=\sqrt{\frac{\sum_{i=1}^{n}\left(\frac{E_{\mathrm{cal}}}{E_{\mathrm{exp}}}-1\right)^2}{n-1}}\times100\% \tag{21}$$

4.3. Modeling analysis of ACP enhanced gas–liquid mass transfer

According to the above description of gas–liquid mass transfer process in the presence of particles, the main parameters affecting the enhancement factor were the distance between particles and gas–liquid interface L, distribution coefficient m, the content of particles m_s, and the residence time of the particles in the gas–liquid interface τ, here the τ can be considered to be equal to the gas–liquid contact time. It is interesting to study the effect of these four parameters on the enhancement factor by using the model established in Section 3.

L is one of the most important factors influencing the enhancement factor of gas–liquid mass transfer. Fig. 11 showed the effect

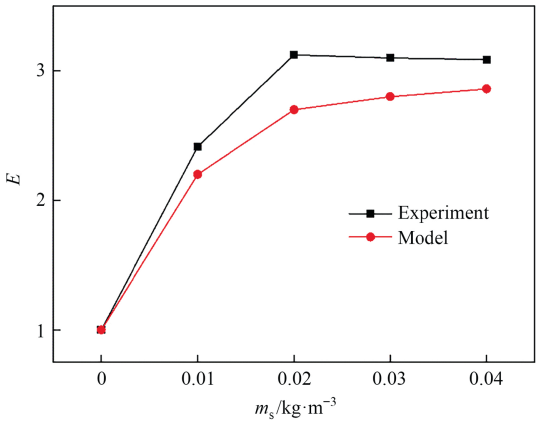

Fig. 8. Comparison of experiment and model for hydrogen absorption in ACP–water system.

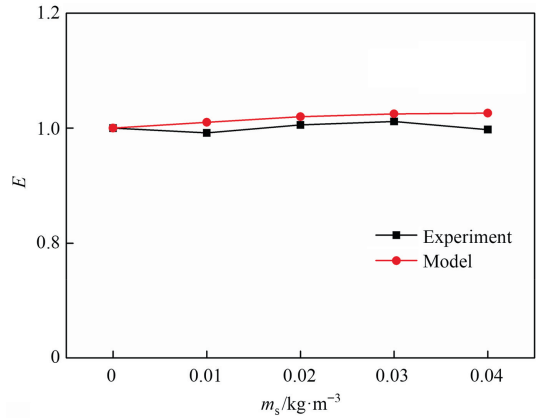

Fig. 9. Comparison of experiment and model for hydrogen absorption in ACP–methanol system.

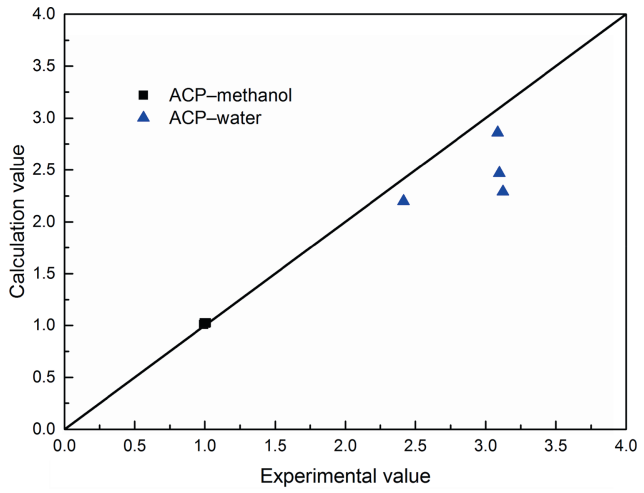

Fig. 10. The comparison of the experiments and calculation.

of L on the enhancement factor by model calculating with the variation of L from 0.5d to 2d. A small value of the L means a short distance between ACP in liquid and gas phase, and the diffusion resistance can be greatly reduced, which are beneficial to the mass

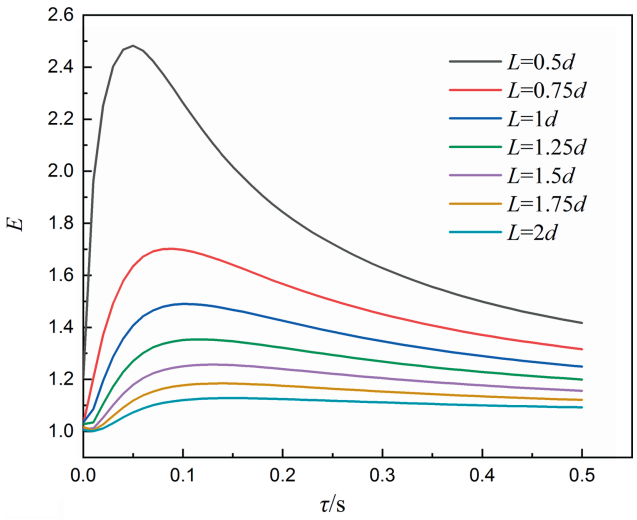

Fig. 11. Effects of the distance L between the particle and gas–liquid interface on the enhancement factor (D_A = 2 × 10^{-9} m^2·s^{-1}, $D_{A,d}$ = 4 × 10^{-10} m^2·s^{-1}, d = 5 μm, m = 100, m_s = 0.35% (mass)).

transfer from gas to liquid phase. Therefore, the smaller the L, the greater the enhancement factor as shown in Fig. 11. It also proved that the adsorption process of ACP is the limiting step when the liquid is in the turbulent state. When the L decreases to a certain value, the diffusion resistance between ACP and gas can be neglected, corresponding to the sharp increase of enhancement factor at the beginning. On the contrary, when the diffusion distance L is large, it takes a long time for the gas diffusing to contact the ACP, and thus, the enhancement factor increases more slowly with the increase of the residence time. In Fig. 11, it was noted that when L decreases to 0.5d, the enhancement factor represents the most drastically increasing trend with reference time increase at the beginning, in which the maximum enhancement factor up to 2.5 could be obtained. When L is twice the ACP diameter d, the enhancement factor represents the most slightly increasing trend, in which the maximum enhancement factor is only about 1.1. Moreover, the residence times corresponding to the maximum enhancement factor were shown to increase with the increase of L in Fig. 11. For example, it was observed as 0.05 s at L of 0.5d and 0.12 s at L of 2d, respectively, this is because the time required for ACP to reach saturation becomes longer due to the slower process for the gas diffusing to contact the ACP as discussed above.

The distribution coefficient m refers to the solute partitioning between the solid particles and the liquid phase [12], which reflects the adsorption capacity of the particles in liquid. A larger distribution coefficient usually means a greater adsorption capability for solute by particles, and consequently, a longer time is needed to achieve the saturated state of the particles. Fig. 12 showed the effect of different distribution coefficient on the enhancement factor by varying the m from 1 to 200. It was illustrated that a larger distribution coefficient results in a higher enhancement factor. Additionally, it should be pointed out that, in Fig. 11, and Fig. 12, there are some minor differences between the starting values, which are caused by the rapid changes at the beginning of the residence time under different operating conditions based on the model calculation.

Fig. 13 showed the effect of particle concentration on the enhancement factor. It was demonstrated that the increasing rate of enhancement factor is more rapid with a high content of ACP at the beginning of the reference time. It was noted that with the increase of ACP content, the residence time required to reach the maximum enhancement factor becomes shortened. This is because

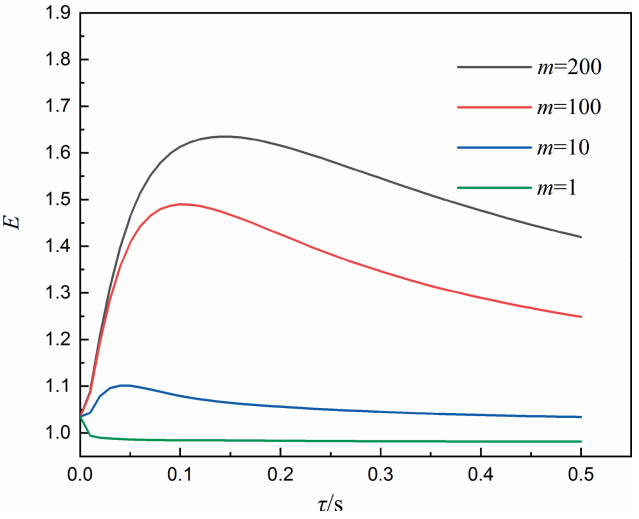

Fig. 12. Effects of the distribution coefficient on the enhancement factor (D_A = 2 × 10^{-9} m^2•s^{-1}, $D_{A,d}$ = 4 × 10^{-10} m^2•s^{-1}, d = 5 μm, L = d, m_s = 0.35% (mass)).

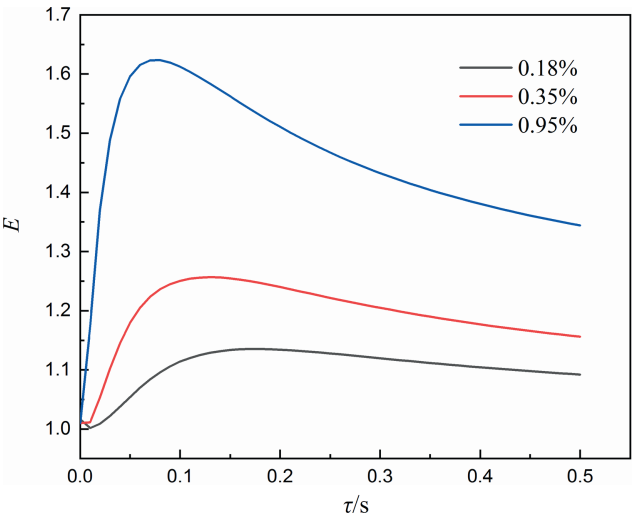

Fig. 13. Effects of particle mass concentration on the enhancement factor (D_A = 2 × 10^{-9} m^2•s^{-1}, $D_{A,d}$ = 4 × 10^{-10} m^2•s^{-1}, d = 5 μm, L = $\delta x/2$, m = 100).

the model is a single particle model, which means a larger ACP concentration leads to a smaller calculation area. With increasing the content of ACP, L becomes small, and thus, the saturation state is easier to be reached.

It was also observed from Figs. 11–13 that all the enhancement factors increase up to a maximum and then decrease with the increase of residence time. This phenomenon can be explained by the following point of view. Before the ACP reach the saturated state, the absorption capacity of the ACP is higher than that of the solvent, presented as the enhancement of mass transfer. After the ACP reach the saturated state, the ACP can no longer adsorb the components, and thus the enhancement effect disappears gradually. Therefore, after the residence time exceeds the time when the ACP reach the saturated state, the enhancement factor will decrease as the time continues.

5. Conclusions

In this paper, we proposed a route of study on the absorption performance of gas into liquid containing solid particles in a stirred constant temperature reactor. A measuring device for gas solubility was built, and a calculation method for the liquid volume mass transfer coefficient was established. It was revealed that ACP can increase the mass transfer coefficient by about three times in the ACP–water system, while in the ACP–methanol system, this effect turned out to be very little and can be ignored. With the increase of ACP content in water, both the mass transfer coefficient and the enhancement factor increase rapidly up to a maximum, and then tends to level. Based on the shuttle effect and two-film theory, a three-dimensional unsteady heterogeneous mass transfer model was also established. The effects of the distance between the particle and the gas–liquid interface L, the distribution coefficient m, the content of ACP m_s, and the residence time τ on the enhancement factor E were all analyzed by modeling calculation. It was found that E decreases with the increase of L, when L is more than 2 times the particle diameter, the enhancement factor is close to 1, and the ACP could hardly enhance the gas–liquid mass transfer coefficient; the enhancement factor increases with the increase of m, and when the m is less than 10, the enhancement of the ACP to the mass transfer coefficient can be ignored; the enhancement factor increases as the content of ACP increase; E increases first and then decreases as the residence time increases. The total standard deviation (SD) was shown to be only 7.78%, indicating a good agreement between the calculation and experimental results.

Declaration of Competing Interest

The authors declare that they have no known competing financial interests or personal relationships that could have appeared to influence the work reported in this paper.

Acknowledgements

This work was supported by National Key Research and Development Program of China (2019YFA0210302), the National Natural Science Foundation of China (21878009, 21901141), and Basic Research Plan for Public Welfare of Zhejiang Province, China (LZY21B060001).

Nomenclature

c^*	liquid phase concentration in equilibrium with gas pressure, mol•m^{-3}
c_A	concentration of components to be transferred in the continuous phase, mol•m^{-3}
$c_{A,\,d}$	concentration of components to be transferred in the dispersed phase, mol•m^{-3}
c_L	concentration of components to be transferred in the liquid bulk, mol•m^{-3}
c_{Li}	concentration of components to be transferred at the gas–liquid interface, mol•m^{-3}
D_A	diffusion coefficient in continuous phase, m^2•s^{-1}
$D_{A,d}$	diffusion coefficient in dispersed phase, m^2•s^{-1}
D_0	diffusion coefficient in blank base solution, m^2•s^{-1}
d	particles diameter, m
E	enhancement factor
k_a	particles adhesion coefficient, m^3•kg^{-1}
k_La	liquid volume mass transfer coefficient, s^{-1}
m	distribution coefficient
m_s	content of particles in suspension, kg•m^{-3}
N_G	amount of components to be transferred in the gas phase, mol
N_L	amount of components to be transferred in the liquid phase, mol
p_f	partial pressure of hydrogen in the equilibrium chamber after equilibration, Pa

p_i	partial pressure of hydrogen in the equilibrium chamber after inflation, Pa
p_0	pressure in the equilibrium chamber before inflation, Pa
p_1	pressure in the equilibrium chamber after inflation, Pa
p_2	pressure in the equilibrium chamber after equilibration, Pa
R	ideal gas constant
T	temperature, K
V_G	volume of the gas phase in the equilibrium chamber, m^3
V_L	volume of the liquid phase in the equilibrium chamber, m^3
ε	turbulent energy dissipation rate, $W \cdot kg^{-1}$
μ	dynamic viscosity, Pa•s
τ	residence time, s
υ	kinematic viscosity, $m^2 \cdot s^{-1}$
Φ_s	volume fraction of dispersed phase at gas–liquid interface
$\Phi_{s,max}$	maximum volume fraction of dispersed phase at gas–liquid interface

References

[1] Y.K. Kim, S.E. Park, H. Lee, J.Y. Yun, Enhancement of bioethanol production in syngas fermentation with Clostridium Ljungdahlii using nanoparticles, *Bioresour. Technol.* 159 (2014) 446–450.

[2] Y.K. Kim, H. Lee, Use of magnetic nanoparticles to enhance bioethanol production in syngas fermentation, *Bioresour. Technol.* 204 (2016) 139–144.

[3] Á. O'Driscoll, J.J. Leahy, T. Curtin, The influence of metal selection on catalyst activity for the liquid phase hydrogenation of furfural to furfuryl alcohol, *Catal. Today* 279 (2017) 194–201.

[4] R.M. Mironenko, O.B. Belskaya, T.I. Gulyaeva, M.V. Trenikhin, A.I. Nizovskii, A.V. Kalinkin, V.I. Bukhtiyarov, A.V. Lavrenov, V.A. Likholobov, Liquid-phase hydrogenation of benzaldehyde over Pd-Ru/C catalysts: Synergistic effect between supported metals, *Catal. Today* 279 (2017) 2–9.

[5] S. Srivastava, G.C. Jadeja, J. Parikh, Copper–cobalt catalyzed liquid phase hydrogenation of furfural to 2-methylfuran: An optimization, kinetics and reaction mechanism study, *Chem. Eng. Res. Des.* 132 (2018) 313–324.

[6] G.A. Filonenko, W.L. Vrijburg, E.J.M. Hensen, E.A. Pidko, On the activity of supported Au catalysts in the liquid phase hydrogenation of CO_2 to formates, *J. Catal.* 343 (2016) 97–105.

[7] J.T. Tinge, A.A.H. Drinkenburg, Absorption of gases into activated carbon–water slurries in a stirred cell, *Chem. Eng. Sci.* 47 (6) (1992) 1337–1345.

[8] E. Alper, B. Wichtendahl, W.D. Deckwer, Gas absorption mechanism in catalytic slurry reactors, *Chem. Eng. Sci.* 35 (1–2) (1980) 217–222.

[9] O. Ozkan, A. Calimli, R. Berber, H. Oguz, Effect of inert solid particles at low concentrations on gas–liquid mass transfer in mechanically agitated reactors, *Chem. Eng. Sci.* 55 (14) (2000) 2737–2740.

[10] R.L. Kars, R.J. Best, A.A.H. Drinkenburg, The sorption of propane in slurries of active carbon in water, *Chem. Eng. J.* 17 (3) (1979) 201–210.

[11] K.C. Ruthiya, B.F.M. Kuster, J.C. Schouten, Gas–liquid mass transfer enhancement in a surface aeration stirred slurry reactors, *Can. J. Chem. Eng.* 81 (3–4) (2008) 632–639.

[12] J.F. Demmink, A. Mehra, A.A.C.M. Beenackers, Gas absorption in the presence of particles showing interfacial affinity: Case of fine sulfur precipitates, *Chem. Eng. Sci.* 53 (16) (1998) 2885–2902.

[13] J.F. Demmink, A. Mehra, A.A.C.M. Beenackers, Absorption of hydrogen sulfide into aqueous solutions of ferric nitrilotriacetic acid: Local auto-catalytic effects, *Chem. Eng. Sci.* 57 (10) (2002) 1723–1734.

[14] M.V. Dagaonkar, H.J. Heeres, A.A.C.M. Beenackers, V.G. Pangarkar, The application of fine TiO_2 particles for enhanced gas absorption, *Chem. Eng. J.* 92 (1–3) (2003) 151–159.

[15] D.W.F. Brilman, W.P.M. van Swaaij, G.F. Versteeg, A one-dimensional instationary heterogeneous mass transfer model for gas absorption in multiphase systems, *Chem. Eng. Process. Process. Intensif.* 37 (6) (1998) 471–488.

[16] G.D. Zhang, W.F. Cai, C.J. Xu, M. Zhou, A general enhancement factor model of the physical absorption of gases in multiphase systems, *Chem. Eng. Sci.* 61 (2) (2006) 558–568.

[17] E. Brunner, Solubility of hydrogen in 10 organic solvents at 298.15, 323.15, and 373.15 K, *J. Chem. Eng. Data* 30 (3) (1985) 269–273.

[18] H. Vinke, P.J. Hamersma, J.M.H. Fortuin, Enhancement of the gas-absorption rate in agitated slurry reactors by gas-adsorbing particles adhering to gas bubbles, *Chem. Eng. Sci.* 48 (12) (1993) 2197–2210.

[19] G. Batchelor, The Theory of Homogeneous Turbulence, 2nd ed., Cambridge University Press, Cambridge, 1971.

[20] E. Nagy, T. Feczkó, B. Koroknai, Enhancement of oxygen mass transfer rate in the presence of nanosized particles, *Chem. Eng. Sci.* 62 (24) (2007) 7391–7398.

[21] G.I. Taylor, The viscosity of a fluid containing small drops of another fluid, *Proc. R. Soc. Lond. A* 138 (834) (1932) 41–48.

[22] M.V. Dagaonkar, H.J. Heeres, A.A.C.M. Beenackers, V.G. Pangarkar, Investigation of enhanced gas absorption by adsorptive bucky balls in a multiphase slurry reactor in the presence and absence of ultrasound, *Ind. Eng. Chem. Res.* 41 (6) (2002) 1496–1503.

[23] O.J. Wimmers, J.M.H. Fortuin, The use of adhesion of catalyst particles to gas bubbles to achieve enhancement of gas absorption in slurry reactors—II. Determination of the enhancement in a bubble-containing slurry reactor, *Chem. Eng. Sci.* 43 (2) (1988) 313–319.